

Directly Visualizing Tactile Perception and Ultrasensitive Tactile Sensors by Utilizing Body-Enhanced Induction of Ambient Electromagnetic Waves

Zewei Ren, Jinhui Nie, Liang Xu, Tao Jiang, Baodong Chen, Xiangyu Chen,*
and Zhong Lin Wang*

Tactile recognition is a critical technology for many applications. Here, it is found that the ambient electromagnetic signal, which is usually regarded as electromagnetic noise, can be a good triggering source to realize tactile detection. A circuit consisting of two light emitting diodes (LEDs) is designed as sensor unit and human contact can amplify the electrostatic signal induced by electromagnetic wave in this circuit, which enhances the brightness of the LEDs. Hence, visualizing tactile perception can be achieved based on this strategy. Accordingly, a stretchable and semi-transparent sensor matrix is established for mapping detailed contact positions, on which the contact force can be smaller than 0.001 N. The detection and the visualization of sliding trajectory and pressure change are also demonstrated by using this sensory method, indicating its good applicability for different purposes. Electromagnetic wave universally exists in the working places and tactile sensors based on this strategy can be possibly applied to many fields such as factory automation, intelligent robotics, human-machine interaction, etc.

A high-performance tactile sensor can be applied to a variety of technologies, such as security monitoring, industrial automation, intelligent robotics, electronics skin and so on.^[6–10] With the emergence of various functional materials, many novel characteristics of high stretchability, self-healing or self-powered capabilities have also been applied to tactile sensors.^[11–14] In addition to the material innovation, many different physical mechanisms have also been employed as transduction principle of tactile sensors, including piezoresistivity, variable capacitance, and even contact-electrification effect.^[10,15–20] The introduction of different physical mechanisms can further stimulate the development of high-performance tactile sensor. For example, in 2013, the visualized pressure mapping has been demonstrated by applying the piezophototronic effect to modulate the light-emitting performance

1. Introduction


Mimicking human sensing by using electronic system is a critical component for artificial intelligence and human-machine interactions.^[1,2] Among all the human senses, a great deal of effort have been focused on realizing tactile perception, which is a more challenging task in comparison with other senses.^[3–5]

of a ZnO nanowire array and an unprecedented spatial resolution of 2.7 mm was achieved.^[21] The key target of tactile sensory technique in the industrial field is to achieve both high resolution and high sensitivity while to simplify the complexity of the system. Therefore, the constant experimentation of different transduction mechanisms for realizing tactile perception is a necessary task for the development of tactile sensor, which can boost the applications in the fields of smartphones, human-machine interaction, etc.

In the past few years, sensory technique based on Maxwell's displacement current and electrostatic field has drawn significant attentions as a newly emerged study direction.^[22,23] The induction-type sensor based on tribo-electric nanogenerators (TENG) is one of the most representative techniques for utilizing Maxwell's displacement current. These TENG-based sensors can generate a large voltage output to enhance the sensitivity of detection and reduce the energy consumption at the same time. However, the electrostatic field generated by TENG decreases quickly due to the leakage and ion neutralization, which would increase the complexity of data acquisition system. The mapping resolution of these TENG-based sensors may also be jeopardized by cross-induction effect induced during contact electrification.^[24–27] Therefore, it is highly desirable to develop a modified method that can carry forward the advantages of these TENG-based sensors and avoid their defects. During the study of TENG-based sensors, we have found that the ambient

Z. Ren, J. Nie, Dr. L. Xu, Dr. T. Jiang, Dr. B. Chen, Prof. X. Chen,
Prof. Z. L. Wang
Beijing Institute of Nanoenergy and Nanosystems
Chinese Academy of Sciences
Beijing 100083, China
E-mail: chenxiangyu@binn.cas.cn; zhong.wang@mse.gatech.edu

Z. Ren, J. Nie, Dr. L. Xu, Dr. T. Jiang, Dr. B. Chen, Prof. X. Chen,
Prof. Z. L. Wang
School of Nanoscience and Technology
University of Chinese Academy of Sciences
Beijing 100049, China
Prof. Z. L. Wang
School of Material Science and Engineering
Georgia Institute of Technology
Atlanta, GA 30332-0245, USA

 The ORCID identification number(s) for the author(s) of this article can be found under <https://doi.org/10.1002/adfm.201805277>.

DOI: 10.1002/adfm.201805277

electromagnetic wave can induce voltage signal in the TENG system. In view of the above facts, we are inspired to use electromagnetic wave as the trigger signal to realize a different induction-type tactile sensor.

In this work, we have designed a very simple circuit that consists of two serially connected light emitting diodes (LEDs) to work as the sensing unit for tactile sensor system, where electromagnetic wave is utilized as the triggering signal. The electromagnetic wave can induce electrostatic signal on human body and the signal can be brought into the sensor circuit when human finger contacts with the sensing node. The non-linear current–voltage characteristic of LEDs can be used to detect the presence of an AC electromagnetic signal at the contact point. Hence, the contact behavior can be visualized by the brightness change from LEDs. We have demonstrated three kinds of tactile sensors that can detect and visualize the contact positions, sliding trajectory and pressure change. The electromagnetic wave and irradiation universally exist in our working environment, especially in the office and factory, which can provide a continuous triggering signal for this sensor. The simple design of this LED sensor unit not only reduces the fabrication cost but also brings a different approach for achieving high-sensitive, high-resolution, and visualized tactile sensors.

2. Results and Discussion

Figure 1a shows the basic working principle of this tactile sensor device. The sensor unit consists of two LEDs connected in series and a contacting node made by conductive materials that has

been inserted at the middle position of two LEDs. Meanwhile, the sensor circuit is connected to the grounded position (see Figure 1a), in order to establish a discharge outlet for the electromagnetic signal. When the absorbing mediums (such as human body) are connected to the ground, ambient electromagnetic wave can induce electrostatic signal on the medium, as is shown in Figure 1a. Hence, the similar electrostatic signal can also be induced in the LED sensor circuit when the contacting node is touched by human body. Then, the current signal in the circuit can show significant enhancement in response to the excitation of electrostatic signal. Meanwhile, the light signal from two LEDs can also be changed with the change of current, which can be used to realize the visualized tactile perception. The working performance of this sensor device touched by human finger can be seen in Figure 1b and Movie 1, where the enhancement of current signal can be clearly presented by the brightness of LEDs. Here, three pure dry batteries are applied as the DC power source for the circuit, in order to avoid influence from instruments of power source. The working mechanism of this induction effect excited by electromagnetic wave can be compared with the working principle of a single-electrode TENG,^[28] which is shown in Figure S1a in the Supporting Information. The contact electrification generates surface charges on the dielectric and the reciprocating motion of the dielectric can induce periodic potential changing on the electrode. Accordingly, the charges are attracted from ground to the electrode, in order to screen the electrostatic potential. The typical I – V performance of single-electrode TENG is also shown in Figure S1a (Supporting Information), where the increase of different external resistance results in the decrease of output current and the increase of output voltage. When human

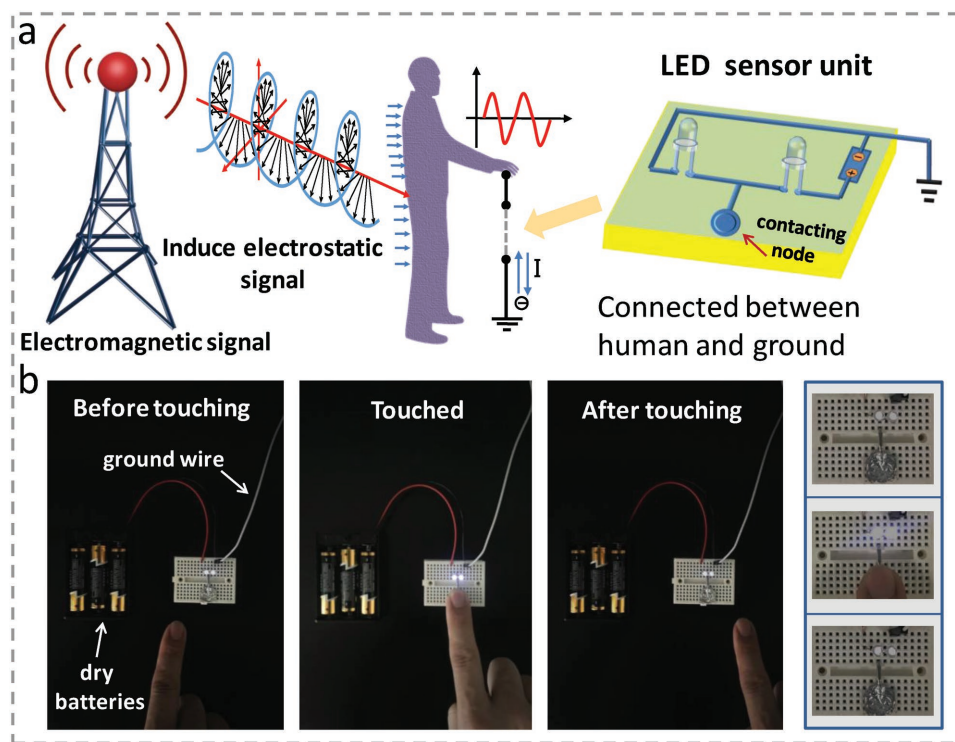


Figure 1. Overview of the LED sensor device. a) Schematic diagram and working mechanism of the device. b) Brightness change of LEDs when contacting node is touched by human motion.

body encounters electromagnetic wave, the periodic electrostatic potential change can also be induced on body. Similarly, the charge from ground can be attracted to human body to compensate potential change, which can generate displacement current from ground to human hand, as can be seen in Figure S1b. This induction process can be measured by using electrometer, as can be seen in Figure S1c–e. The electrometer is connected between the ground and human hand, while positive electrode of the electrometer is connected to human hand and the negative electrode of the electrometer is grounded. With the increase of the connected resistance, the generated displacement current decreases and the established output voltage increases, which is the same as typical I - V performance of single-electrode TENG. Here, the open-circuit voltage induced by human finger is about 6.5 V and the short-circuit current is about 0.25 μ A. It is important to note that the induced energy generation from electromagnetic signal is much smaller than the common output from TENG, but it can provide a rather constant triggering source with much higher sensitivity. The changing frequency of this induced electrostatic signal is also quite high in comparison with common TENG, which is in accordance with the electromagnetic signal generated by the surrounding electrical equipment.

For the operation of tactile sensor, the pure resistor is replaced by LED sensor circuit, as shown in Figure 1a. The I - V characteristic of two serially connected LEDs is shown in Figure S2a. During the operation, stable voltage signal of 4.8 V is applied on the two serially connected LEDs. At this voltage, the channel inside the LED is not fully opened, but it is very close to the threshold value (around 5 V). Since LED is non-linear device with exponential property, the slight increase of voltage at this value can generate huge current increase (Figure S2a). Hence, tiny electrostatic excitation induced by the electromagnetic wave is enough to trigger the sensor circuit. In order to check the reaction of linear device to electromagnetic

wave, we replace the LEDs with common resistors (100 K Ω) in the same circuit, as shown in Figure S2b. Since resistor is stable linear component, the average value of the current is unchanged, while the amplitude of the noise signal is severely enhanced by the contact motion. Hence, we confirm that the key point for this sensor circuit is that the LEDs are working at the edge of the threshold voltage and tiny excitation from electromagnetic signal can induce significant enhancement of current, as shown in Figure S2c. The light signal from LEDs is proportional to its current value and therefore, the contact motion can be visualized by this simple sensor unit. The high-speed camera has been used to catch the light signal of two serially connected LEDs, which can be seen in Figure S4 and Movie 2. Two LEDs flash alternatively in response to electromagnetic signal and the flash frequency is higher than that can be distinguished by human eyes. This observation is also in good agreement with electrical measurement. It is important to note that the components in each sensor unit need to be as few as possible, in order to realize a simple and effective tactile sensory system. The circuit with only one LED may also react to the electromagnetic signal, but it cannot fully utilize the AC signal induced by electromagnetic wave. Hence, this double LED circuit is the optimized sensor unit with minimum components and superior sensitivity.

To provide in-depth study of this LED sensor unit, aluminum (Al) foils with different sizes are selected as the absorbing medium for electromagnetic wave, schematic diagram of which is illustrated in Figure 2a. The similar design has been studied by many electric/electronics researchers for harvesting electromagnetic energy.^[29,30] However, for this kind of antenna harvester, the voltage output induced by electromagnetic wave is usually too small to support a sophisticated energy collecting circuit, which strongly suppresses its efficiency. On the other hand, using body-enhanced electromagnetic wave to trigger the

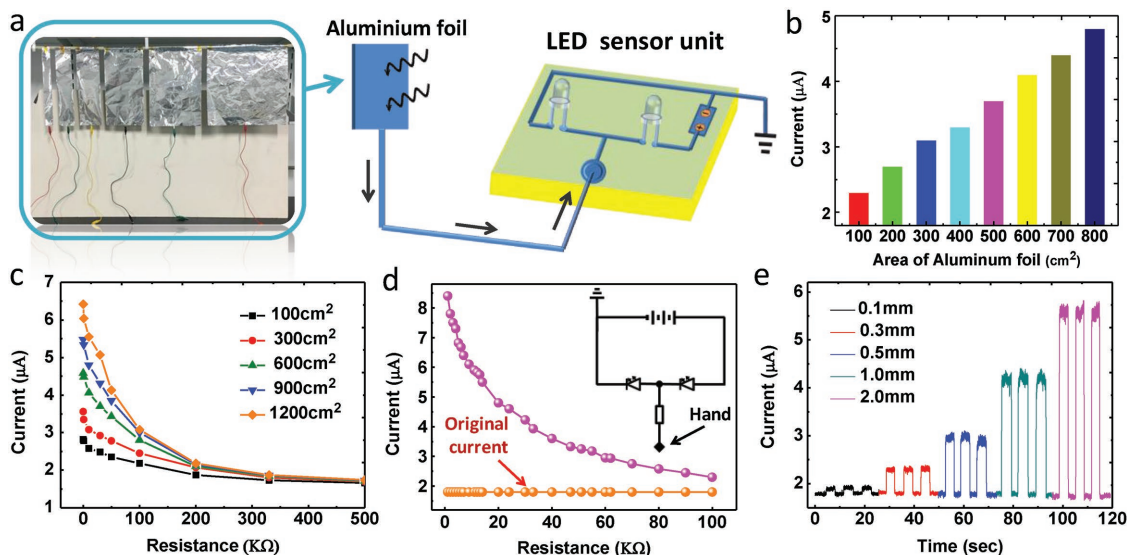


Figure 2. Output characteristics of the sensor device. a) Photograph of Al foil in different size and schematic diagram of Al foil connected to the sensor circuit. b) Current change of the sensor circuit with the connected Al foil in different size. c) Current signals of the circuit with different resistors connected between Al foil and contacting node. d) Current signals of the circuit with different resistors connected between human hand and contacting node. e) Dynamic currents when contacting nodes in different size are touched by human hand.

tactile sensor is a totally different approach for utilizing electromagnetic energy and all these defects of electromagnetic wave can be avoided. To our best knowledge, this kind of application has not been reported before. Figure 2b shows current change of the sensor circuit with different Al antennas, where current value rises linearly with the increase of the size of Al foil. It is important to note that in the same electromagnetic environment, the intensity of the induced electrostatic signal is determined by the size of Al foil, which is also similar to the working principle of single-electrode TENG. In this experiment, ambient electromagnetic signal is monitored by some commercial electromagnetic wave detectors (Pudibei-620A and LZT-1000, Figure S5a in the Supporting Information). The average amplitude of electromagnetic wave signal is around $2\text{--}3\text{ V m}^{-1}$ in the lab and this value is kept constant during the whole experiment. The amplitude of the electromagnetic signal is influenced by number of electrical instruments in the room, such as lamps, computers or electrical wires and the different levels of ambient electromagnetic wave can influence the current value of this sensor unit (see Figure S5b). However, for a fixed environment, the repeatability of the sensing unit is quite reliable. Meanwhile, even if we stop all the visible electrical instruments in the room, the sensor circuit can still react to the contact motion (see Figure S5b), which indicates that this LED sensor unit is very sensitive to the electromagnetic signal. Figure 2c illustrates current value with different resistors connected between Al foil and contacting node, while the size of Al foil changes from 100 to 1200 cm^2 . When the resistance is larger than 500 $\text{k}\Omega$, the change of the current

is negligible. Furthermore, the resistance dependence of the sensor circuit working with human finger is also studied (see Figure 2d), where resistor is connected between human hand and contacting node. Figure 2e shows dynamic change of the current in this sensor circuit, when contacting nodes with different diameters are applied. The summarized results of current change with different contacting node can be seen in Figure S4c. As shown in Figure 2e, when the diameter of the contacting node is close to 0.1 mm, the current change induced by finger contact is suppressed significantly. In this case, the detection of the contact motion can only rely on the measurement of the detailed current value, while the induced change of the light signal from LEDs is difficult to be distinguished by human eyes. However, it is necessary to point out that the LEDs in our experiment are the cheap and common product in the market (each LED is cheaper than 0.01 EUR). The sensitivity of this sensor device for detecting contact motion is determined by the on/off ratio of the LED, as can be seen in Figure 1c. We believe that with more advanced LEDs that possess better $I\text{--}V$ performance, the sensitivity and the resolution of this sensor unit can be both improved and the minimum diameter of the contacting node can be much smaller than 0.1 mm.

In order to show the applicability of this LED sensor unit, we demonstrate a tactile sensor matrix by coupling this sensing strategy with the stretchable ultrathin conductor. The contacting node matrix has been fabricated by elastomeric film and stretchable electrode, structure design and components of which are shown in Figure 3a. The stretchable electrode is made by combining carbon fiber (CF) and Ag nanowires (AgNWs).

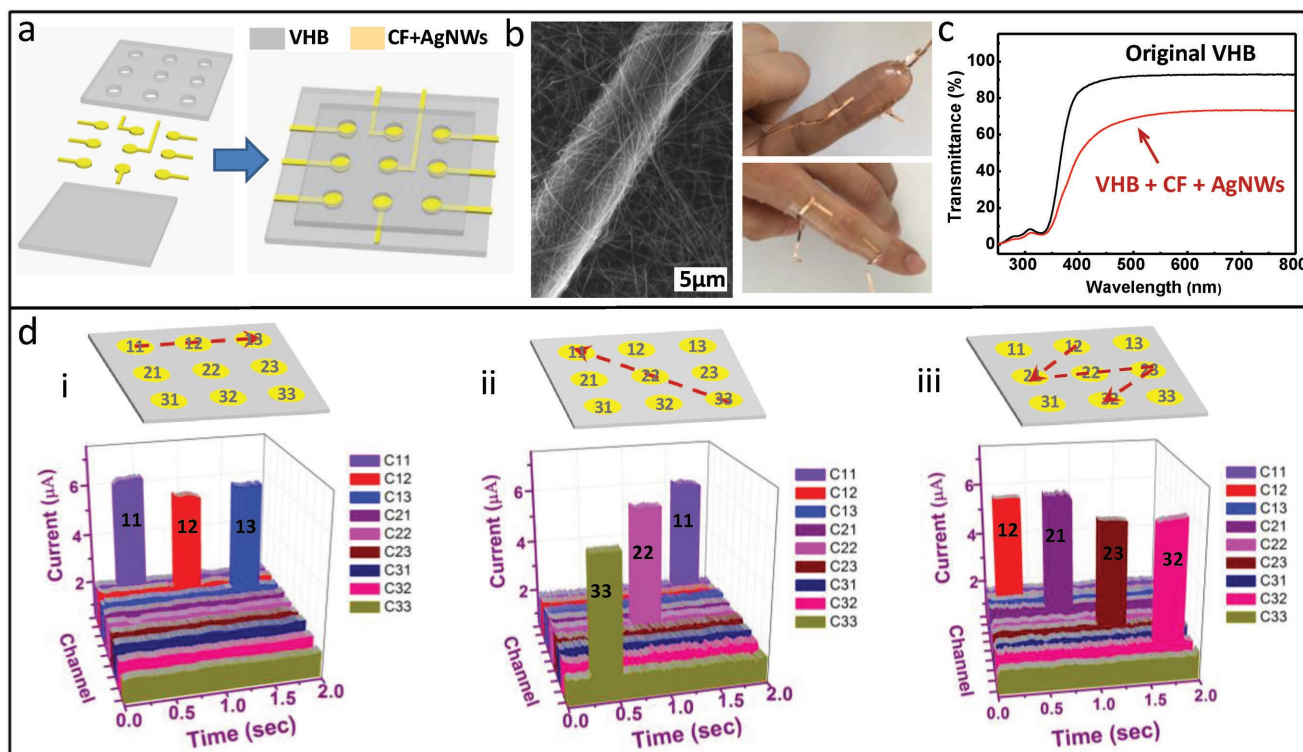


Figure 3. Visualized mapping of touching position with the stretchable sensor matrix. a) Structure design and components of the sensor matrix. b) SEM images of CF–AgNW electrode and photographs of the sensor matrix attached on human finger. c) Transmittances of elastic VHB and AgNW–CF electrode. d) Current signals of nine LED units when contact spots on the matrix are touched by the needle.

The single line of CF is attached on the surface of dielectric elastomer to form the framework of the electrode and then, AgNWs is sprayed on the CF framework to increase the conductivity and the stretchability (the detailed preparation can be found in Figure S6). The commercial Very High Bond (VHB) tape with the thickness of 0.25 mm is selected as the dielectric substrate and the electrode is sealed by another ultrathin VHB film with nine holes as the contact spots. The diameter of contact spot is 1 mm and the area of 3×3 sensor matrix is $6 \text{ mm} \times 6 \text{ mm}$. The nine contact spots in the matrix are respectively connected to nine LED sensor units. This tactile sensor matrix is ultrathin, highly stretchable, semitransparent, and adhesive, which allows it to be easily attached to various substrates, including human skin. Scanning electron microscopy (SEM) images of CF–AgNW electrode and photographs of the sensor matrix attached on human finger are shown in Figure 3b. The related demonstration can be seen in Movies 3 and 4. Figure 3c shows transmittance of VHB film with and without CF–AgNW electrodes. The CF–AgNW electrode on VHB film has a transmittance of 70% (Figure S7) and a resistance of 1–2 K Ω . Furthermore, resistance changes of the CF–AgNW electrode in response to tensile and bending deformation have been elaborated in Figure S8. The resistivity of the CF–AgNW electrode shows only slight increase, when the stretching rate is lower than 25% (Figure S8a,b) or the bending angle is smaller than 60° (Figure S8c,d). The detailed studies related to the AgNW density and its conductivity can be seen in our previous study. Meanwhile, we increased a comparison study about different electrode materials, as can be seen in Table S1. With this sensor matrix, contact positions can be revealed by the current

change in each sensor unit. As exhibited in Figure 3d, when the needle touches the contact spots along the path: (C11) \rightarrow (C12) \rightarrow (C13), currents of corresponding LED units increase dramatically (Figure 3 d(i)). In a similar way, for the sliding path: C33 \rightarrow C22 \rightarrow C11 and C12 \rightarrow C21 \rightarrow C23 \rightarrow C32, the recorded current change of circuits can also clearly reveal the motion of the needle (see Figure 3 d(ii) and (iii)). In this case, tactile behavior can be visually perceived by this stretchable sensor matrix. The design of this sensor matrix is very simple but effective in comparison with most of traditional tactile sensors.^[31] Although some visualized tactile sensors have also been developed by using different physical mechanisms, such as mechanochromic effects, electroluminescent effect^[32–34] or even tribo-electrification effect, the required contact force for these systems is usually much higher than that for our device. Moreover, the complicated logical circuit and the analyzing software is also necessary for these systems, which may increase the cost and the complexity. It is worth noting that the materials of this sensor matrix can be freely replaced and the density of contact spots matrix can be increased by more advanced fabrication process, which can further improve the effectiveness of this sensing method.

Based on this sensing mechanism, an integrated printed circuit board (PCB) has been designed to work as a more sophisticated sensor matrix, as can be seen in Figure 4a. The PCB circuit with 64 (8×8) tiny electrodes as touching nodes is developed to the sensor matrix. Every touching spot in this 8×8 contact matrix is connected to an LED sensor unit and all the sensor units are driven by one power source. The enlarged view of the contact spot matrix is shown in Figure 4a. The

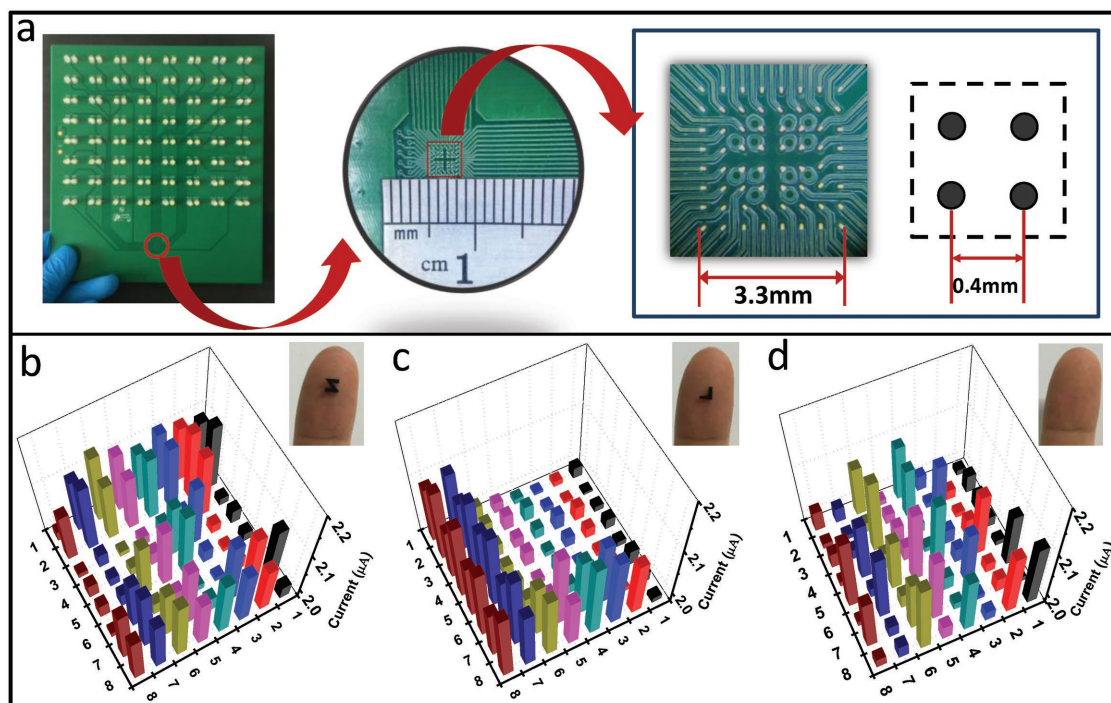


Figure 4. Visualized mapping of touching position with designed PCB. a) Overview of the PCB. b,c) Current signals of 64 LED units and photographs of two tiny conductive objects with the shape of “Z” and “L”. d) Current signals of 64 LED units when the matrix is touched by finger and photograph of the touching finger.

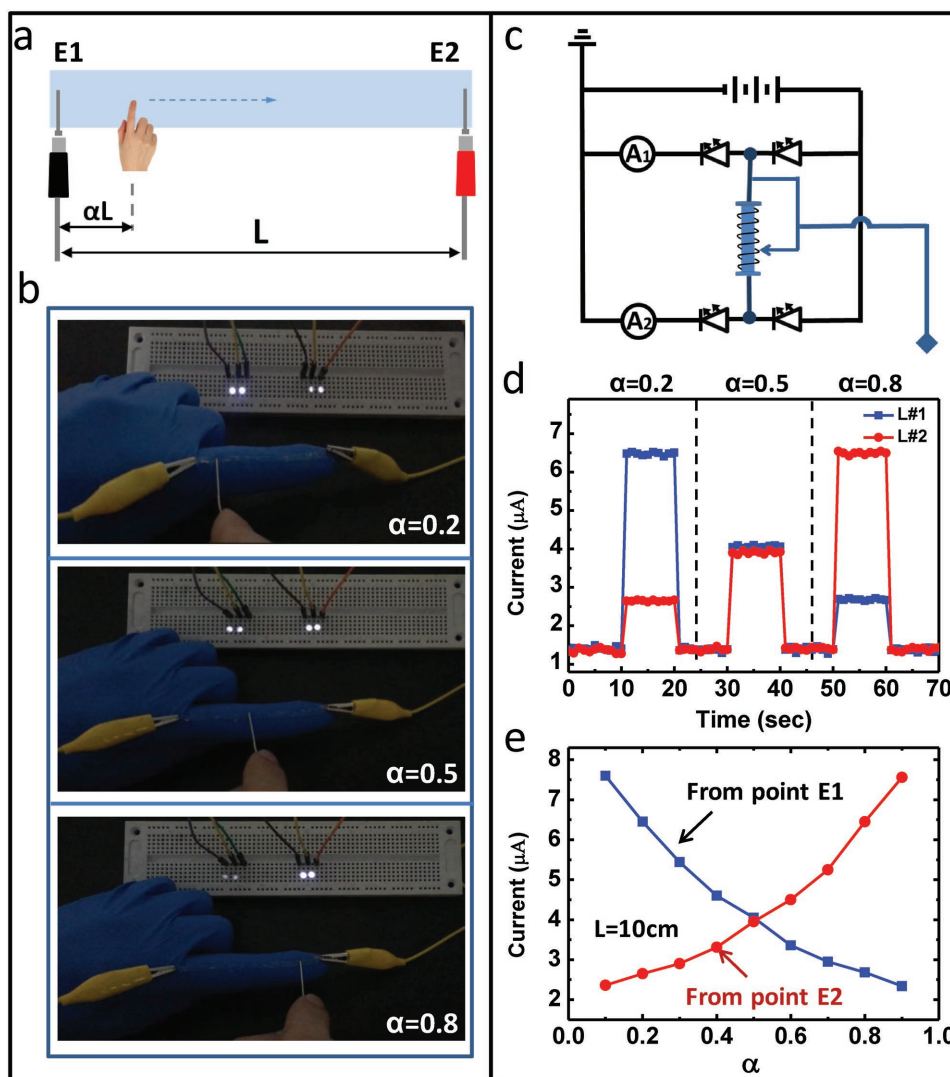


Figure 5. Visualized perception of sliding trajectory with 1D touch strip. a) Schematic diagram of 1D touch strip. b) Light intensity of two LED units when the strip is touched by the clip on different touch points. c) Circuit diagram of the designed tactile sensor. d) Current changes of two sensor circuit in response to touching. e) Currents of two sensor circuits when the strip is touched by the clip from E1 to E2.

diameter of each contact spot is 0.1 mm, the center distance of two neighboring spots is 0.4 mm and the overall dimension of the matrix is 3.3 mm × 3.3 mm. The visualized perception of contact positions can be demonstrated by needle pouncing, as shown in Movie 5. In addition, the shape of different contacting objects can also be recognized by this sensor matrix. Here, two tiny conductive objects with the patterned shape of “Z” and “L” are prepared. The patterned objects are made by mixing polydimethylsiloxane (PDMS) and carbon black (CB) at a mass ratio of 10:1.3 with a resistance smaller than 200 Ω and a thickness of 1 mm. Then, the touching matrix on PCB is touched by these tiny patterned objects attached on finger and the current signals of 64 sensor units are shown in Figure 4b,c, respectively. Current change induced by the contact motion can be clearly observed, where the pattern “Z” and “L” can be recognized by reading the current signals from 64 sensor units. Furthermore, the promising application of this sensor matrix

for brief fingerprint detection is demonstrated. Figure 4d shows the current signals of 64 LED units when the touching matrix is contacted by the finger. It can be found that current changes of 64 LED units are dispersed in space and the fluctuation of current values can be observed. This is caused by the rugged skin lines on the finger, which can alter the detailed contact area between the finger and the sensor matrix. This result can be a simple demonstration of the identification of fingerprint by using this sensor strategy.

The tactile sensor that can visualize the sliding trajectory has been realized by coupling a hydrogel strip and two LED sensor units, as shown in Figure 5a. The hydrogel strip is connected to two LED sensor units on both ends (E1 and E2). When fingers or other conductive objects touch the hydrogel strip, electromagnetic wave can simultaneously induce electrostatic signal in two sensor units. Here, the strip of hydrogel is worked as a sliding rheostat, while the touching position can decide the

resistances assigned to two LED sensor units. The two sensor circuits are connected in series with the hydrogel strip, the corresponding circuit diagram of which is shown in Figure 5c. A normalized distance αL is used to represent the position of the touch point, where L (10 cm) is the length of the hydrogel strip. The left- and the right-hand ends of the strip correspond to $\alpha = 0$ and 1, respectively. The resistance of two developed resistors can be represented by the following equations:

$$R_1 = \alpha R \quad (1)$$

$$R_2 = (1 - \alpha) R \quad (2)$$

where R_1 and R_2 are the resistances measured from two ends of the strip E1 and E2 to the touching point, respectively. R is the resistance of the whole hydrogel strip from E1 to E2, which is around 60 k Ω . The current signals corresponding to different touching positions are shown in Figure 5d and the brightness change of LEDs can be seen in Figure 5b and Movie 6. The current changes of two sensor circuits when the touching position on the strip moving from E1 to E2 are shown in Figure 5e (the position change is 1 cm each time). As the touching point moves from left (E1) to the right (E2), the light intensity (the current) of the left LEDs is weakened, while the light intensity (the current) of the right LEDs is enhanced. Hence, by monitoring the light intensity or the current change of LEDs, the touching position and sliding trajectory in one dimension can be detected and visualized. Based on this simple sensory strategy, a lot of continuous works can be developed to improve the design of many existed trajectory detectors.

By coupling a pressure sensitive conductor with this LED sensor unit, visualized perception of the contacting force and pressure can be realized. The detailed structure design is shown in Figure 6a. This pressure sensitive conductor is made by mixing PDMS and CB. The SEM images of micro-morphology of the PDMS-CB film can be seen in Figure S9a. The elastic properties and conductivity change of this mixed conductive material under different strain are shown in Figure S9b. For the strain lower than 100%, the resistance change of the material is very small and the deformation is also elastic, which demonstrates both good conductivity and tensile strength of this mixed material. The PDMS-CB film has been modified with mini porous structure and sealed by another ultrathin film. Figure 6b exhibits the microscopic image of the porous structure of the PDMS-CB film, which can enhance the compressibility and the sensitivity of conductance changing under different pressures. Photographs of the PDMS-CB film can be seen in Figure 6c,d. The resistance change of this pressure sensitive conductor in response to different pressure is shown in Figure 6e, which illustrates that the resistance will be unchanged with a pressure lower than 1.7 KPa. The resistance change is determined by the deformation of the conductor and the deformation is hardly occurred with such small pressure. In this case, detection of small pressure purely by the resistance change of the conductor may be not possible. However, by coupling the pressure sensitive conductor with the LED sensor unit, the tiny finger touch with the force smaller than 0.001 N would still be detected. More importantly, the pressure changing can be visualized by the brightness change of the

LEDs. The corresponding circuit diagram of the designed tactile sensor is shown in Figure S9c. Figure 6f demonstrates current value change of the LEDs when the conductor is touched by the finger with different pressures (original current is the current without touching). It shows that current change of the circuit can be divided into two processes: first, a dramatic change of the current is induced when the conductor is slightly touched by the finger, where the force applied by the finger in this process is very small or negligible; secondly, with the increase of applied touch force, the current value of the circuit increases continuously since resistance of the conductor decreases. Correspondingly, the brightness change of the LEDs also has two distinct processes, as can be seen in Movie 7. Meanwhile, in order to confirm that the tiny contact force can be detected by the change of light signal of LEDs, a piece of Al foil attached on the sensing area of dynamometer is selected as the contacting node of the LED sensor circuit. The digital change of dynamometer and the brightness change of LEDs under the tiny finger contact can be seen in Movie 8. Photographs of the digital change of the dynamometer and brightness change of LEDs before and after the finger contact can be seen in Figure 6g,h, respectively, where the tiny contact force (<0.001 N) can be visually detected by this sensor unit. In the Figure 6h, 0.001 N is the limit of the dynamometer in our lab. Theoretically, the required contact force for triggering this sensor unit can be zero. Figure 6i shows continuous change of the current value in the sensor circuit with the increase of applied pressure. The combination of pressure sensitive conductor and this sensor unit can realize the visualized observation of the applied pressure. It is necessary to note that detailed current value of the sensor unit may be changed for the different electromagnetic conditions. Accordingly, the pressure detection using this sensor unit can be influenced if the electromagnetic condition is not constant. On the other hand, the applications of this sensor unit for tactile perception, mapping of touching position and trajectory visualization will be rarely affected by environmental factors.

3. Conclusion

In summary, a simple circuit consists of two serially connected LEDs has been designed as the sensor unit to detect various tactile contacts, where ambient electromagnetic signal is working as trigger signal. Electromagnetic wave induces electrostatic signal in this sensor circuit and the contact motion of human or other medium can amplify this induction effect. Then, the exponential property of LEDs leads to the strong enhancement of the current signal under the excitation of electromagnetic signal, where the visualized tactile perception can be realized by observing the brightness change of LEDs. By using this sensor unit, a stretchable and semitransparent sensor matrix has been designed for mapping contact positions. The minimum diameter of the contacting node is around 0.1 mm and the sensor unit can clearly recognize the finger touch with the contact force smaller than 0.001 N. Both the sensitivity and the resolution can be improved by employed some high-level LED devices. Moreover, a hydrogel strip and a pressure sensitive conductor have been employed to work

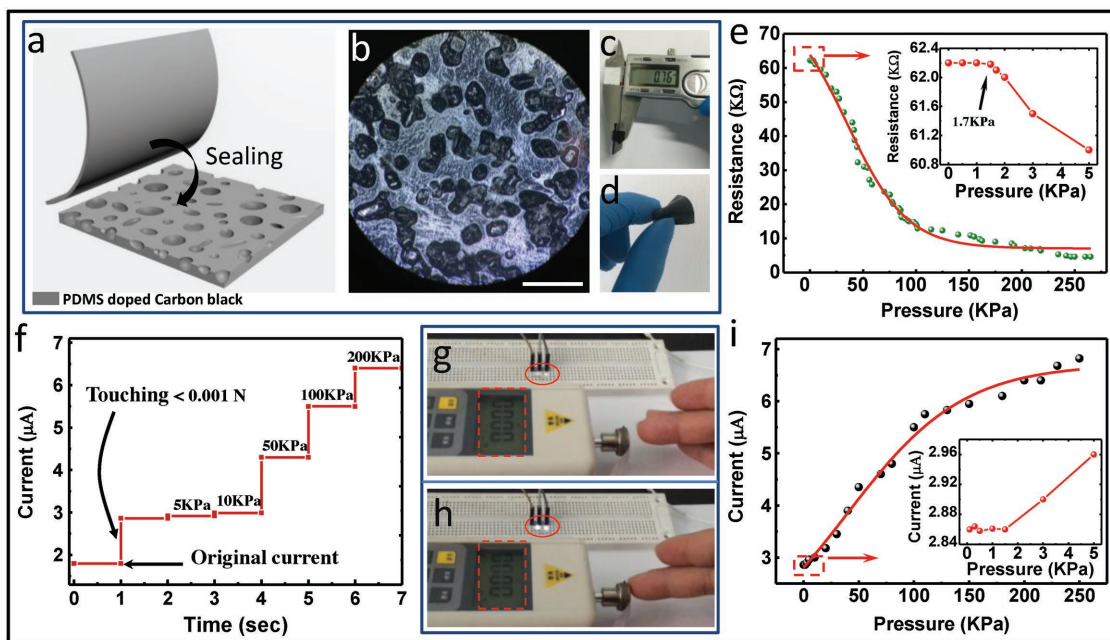


Figure 6. Visualized perception of pressure of the contact with pressure sensitive conductor. a) Structure design and the components of the sheet conductor. b) Microscopic image of the porous structure, the scale bar is 1 mm. c,d) Photographs of the sheet conductor. e) Resistance change of the conductor in response to different pressure. f) Current signals when the conductor is touched by the finger with different pressure. g,h) Photographs of the readings change of the dynamometer and brightness change of LEDs: g) before the Al foil is contacted and h) when the Al foil is contacted. i) Continuous change of the current in the circuit with increasing pressure that applied on the conductor.

together with this sensor unit, which can demonstrate two tactile sensors for detecting and visualizing sliding trajectory and contact pressure. Since electromagnetic wave universally exists in our working places, the continuous operation of these tactile sensors can be realized. Hence, high sensitivity, simple component, and visualization capability of this sensory method can open up various applications in the fields of industrial automation, robotic skins, human-machine interaction, safety monitoring and so on.

4. Experimental Section

Fabrication of the Stretchable and Semitransparent Sensor Matrix: The stretchable sensor matrix is consisted of two stretchable dielectric elastomer films and stretchable electrode that is sandwiched between two elastomer films. The dielectric elastomer of the substrate attached on human skin has a thickness of 250 μm, while the thickness of upper dielectric elastomer for sealing the electrode is only 50 μm. The stretchable electrode is made by AgNW (XFNANO) and CF (SYT45-12K). The diameter of AgNW is 50 nm with length of 100–200 μm and the diameter of CF is 7 μm. The single CF is placed on the surface of dielectric substrate in cross-shapes to form the framework of the electrode and AgNW is sprayed on the CF framework. Finally, the stretchable electrode is sealed by another ultrathin elastomer film. The width of the electrode and the space can be adjusted for different touching objects, since size and shape of the electrode can be controlled by employing some curved masks. The sensor matrix is stretchable, biocompatible, and adhesive, which can be adjusted for different touching objects.

Fabrication of the Hydrogel Strip: The hydrogel is made by acrylamide, LiCl, N,N'-methylenebisacrylamide, ammonium persulfate, and N,N,N',N'-tetramethylethylenediamine. First, acrylamide powder

(14 weight % relative to deionized water) is added into the deionized water. Secondly, N,N'-methylenebisacrylamide (0.0085 weight%), ammonium persulfate (0.0139 weight%) and LiCl (17 weight%) are added into the solution. Finally, N,N,N',N'-tetramethylethylenediamine (0.0347 weight %) is added into the mixed solution. Then, the mixed solution is stirred well with a glass bar and is cured at 60 °C for 2 h in vacuum oven. The strip of hydrogel with the resistance around 60 kΩ and length of 10 cm is acquired. The thickness of the final hydrogel can be controlled by the volume of the solution.

Fabrication of Pressure Sensitive Conductor: The conductor is made by mixing PDMS (Dow Corning, Sylgard 184; ratio of base to cross linker, 10:1 by mass) and CB (TIMICAL SUPER P LI) at a mass ratio of 10:0.8, the original resistance of prepared conductor is around 62.4 kΩ. Since resistance of the mixed PDMS and CB material is determined by the mixing ration of PDMS and CB, the maximum resistance of the conductor can be adjusted. After mixed with CB, the liquid PDMS is poured into the prepared mold and coated with spin coater. Then, the superfine sugar particles are added into the liquid coated film, and the film is vacuumed for 1 h and cured at 80 °C for 1.5 h in vacuum oven. After the film has been cured, it is peeled off slowly from the mold substrate with a tweezer and putted into the deionized water for ultrasonic cleaning. After that, the stretchable conductive film (0.6 mm) with mini porous structure is acquired. To enhance tensile strength of the film, it is sealed by another ultrathin film (0.15 mm) that is made by the same material without mini porous structure inside. In this case, the pressure sensitive conductor with the maximum resistance of 62.4 kΩ and the thickness of 0.76 mm is acquired. The conductor is sheet with a whole dimension of 2 cm × 2 cm.

Supporting Information

Supporting Information is available from the Wiley Online Library or from the author.

Acknowledgements

Z.R. and J.N. contributed equally to this work. This work is supported by the National Key R & D Project from Minister of Science and Technology (2016YFA0202704), Beijing Municipal Science and Technology Commission (Z171100000317001), the “thousands talents” program for pioneer researcher and his innovation team, China, NSFC Key Program (no. 21237003), and National Natural Science Foundation of China (grant nos. 51775049, 51432005, 11674215, 5151101243, and 51561145021).

Conflict of Interest

The authors declare no conflict of interest.

Keywords

electromagnetic waves, tactile sensors, trajectory mapping., tribo-electric nanogenerators, visualized tactile perception

Received: July 31, 2018
Revised: August 30, 2018
Published online:

-
- [1] W. Gao, S. Emaminejad, H. Y. Nyein, S. Challa, K. Chen, A. Peck, H. M. Fahad, H. Ota, H. Shiraki, D. Kiriya, D.-H. Lien, G. A. Brooks, R. W. Davis, A. Javey, *Nature* **2016**, 529, 509.
- [2] C. Larson, B. Peele, S. Li, S. Robinson, M. Totaro, L. Beccai, B. Mazzolai, R. Shepherd, *Science* **2016**, 351, 1071.
- [3] Y. Fu, M. Zhang, Y. Dai, H. Zeng, C. Sun, Y. Han, L. Xing, S. Wang, X. Xue, Y. Zhan, Y. Zhang, *Nano Energy* **2018**, 44, 43.
- [4] L. Wang, H. Peng, X. Wang, X. Chen, C. Yang, B. Yang, J. Liu, *Microsyst. Nanoeng.* **2016**, 2, 16065.
- [5] X. Chen, Y. Wu, J. Shao, T. Jiang, A. Yu, L. Xu, Z. L. Wang, *Small* **2017**, 13, 1702929.
- [6] Q. Sun, D. H. Kim, S. S. Park, N. Y. Lee, Y. Zhang, J. H. Lee, K. Cho, J. H. Cho, *Adv. Mater.* **2014**, 26, 4735.
- [7] Z. Ren, J. Nie, J. Shao, Q. Lai, L. Wang, J. Chen, X. Chen, Z. L. Wang, *Adv. Funct. Mater.* **2018**, 28, 1802989.
- [8] T. Q. Trung, N. E. Lee, *Adv. Mater.* **2016**, 28, 4338.
- [9] Y. Dai, Y. Fu, H. Zeng, L. Xing, Y. Zhang, X. Xue, *Adv. Funct. Mater.* **2018**, 28, 1800275.
- [10] L. Viry, A. Levi, M. Totaro, A. Mondini, V. Mattoli, B. Mazzolai, L. Beccai, *Adv. Mater.* **2014**, 26, 2659.
- [11] Q. Liang, Q. Zhang, X. Yan, X. Liao, L. Han, F. Yi, M. Ma, Y. Zhang, *Adv. Mater.* **2017**, 29, 1604961.
- [12] A. Yu, X. Chen, R. Wang, J. Liu, J. Luo, L. Chen, Y. Zhang, W. Wu, C. Liu, H. Yuan, M. Peng, W. Hu, J. Zhai, Z. L. Wang, *ACS Nano* **2016**, 10, 3944.
- [13] Q. Sun, W. Seung, B. J. Kim, S. Seo, S. W. Kim, J. H. Cho, *Adv. Mater.* **2015**, 27, 3411.
- [14] M. F. Lin, J. Xiong, J. Wang, K. Parida, P. S. Lee, *Nano Energy* **2018**, 44, 248.
- [15] P. Wang, Y. Fu, B. Yu, Y. Zhao, L. Xing, X. Xue, *J. Mater. Chem. A* **2015**, 3, 3529.
- [16] J. Park, Y. Lee, J. Hong, M. Ha, Y. Jung, H. Lim, S. Y. Kim, H. Ko, *ACS Nano* **2014**, 8, 4689.
- [17] X. Chen, D. Taguchi, T. Manaka, M. Iwamoto, *J. Appl. Phys.* **2012**, 111, 113711.
- [18] X. Chen, L. Liu, Y. Feng, L. Wang, Z. Bian, H. Li, Z. L. Wang, *Mater. Today* **2017**, 20, 501.
- [19] A. Damilano, P. M. Ros, A. Sanginario, A. Chiolerio, S. Bocchini, I. Roppolo, C. F. Pirri, S. Carrara, D. Demarchi, M. Crepaldi, *IEEE Sens. J.* **2017**, 17, 2682.
- [20] X. Chen, D. Taguchi, T. Manaka, M. Iwamoto, *Org. Electr.* **2013**, 14, 320.
- [21] C. Pan, L. Dong, G. Zhu, S. Niu, R. Yu, Q. Yang, Y. Liu, Z. L. Wang, *Nat. Photon.* **2013**, 7, 752.
- [22] K. Parida, V. Kumar, J. Wang, V. Bhavanasim, R. Bendi, P. S. Lee, *Adv. Mater.* **2017**, 29, 1702181.
- [23] S. Wang, L. Lin, Z. L. Wang, *Nano Energy* **2015**, 11, 436.
- [24] X. Chen, M. Iwamoto, Z. Shi, L. Zhang, Z. L. Wang, *Adv. Funct. Mater.* **2015**, 25, 739.
- [25] K. Y. Lee, M. K. Gupta, S. W. Kim, *Nano Energy* **2015**, 14, 139.
- [26] Y. Zi, S. Niu, J. Wang, Z. Wen, W. Tang, Z. L. Wang, *Nat. Commun.* **2015**, 6, 8376.
- [27] X. Chen, Y. Wu, A. Yu, L. Xu, L. Zheng, Y. Liu, H. Li, Z. L. Wang, *Nano Energy* **2017**, 38, 91.
- [28] S. Niu, Y. Liu, S. Wang, L. Lin, Y. S. Zhou, Y. Hu, Z. L. Wang, *Adv. Funct. Mater.* **2014**, 24, 3332.
- [29] X. Lu, P. Wang, D. Niyato, D. Kim, Z. Han, *IEEE Commun. Surv. Tutor.* **2015**, 17, 757.
- [30] A. Mavaddat, S. Armaki, A. R. Erfanian, *IEEE Antennas Wireless Propag. Lett.* **2015**, 14, 515.
- [31] X. Wang, H. Zhang, L. Dong, X. Han, W. Du, J. Zhai, C. Pan, Z. L. Wang, *Adv. Mater.* **2016**, 28, 2896.
- [32] M. I. Tiwana, S. J. Redmond, N. H. Lovell, *Sens. Actuators A: Phys.* **2012**, 179, 17.
- [33] Y. Wan, Y. Wang, C. Guo, *Mater. Today Phys.* **2017**, 1, 61.
- [34] F. Juanes, *J. Nat. Conserv.* **2018**, 42, 7.